Properties of Small- to Medium-Sized Mercury Clusters from a Combined *ab initio*, Density-Functional, and Simulated-Annealing Study

Gloria Esperanza Moyano, Ralf Wesendrup, Tilo Söhnel, and Peter Schwerdtfeger
Department of Chemistry, The University of Auckland, Private Bag 92019, Auckland, New Zealand
(Received 19 December 2001; published 15 August 2002)

Relativistic coupled-cluster and second-order many-body perturbation theories were used to construct two- and three-body potentials for the interaction between mercury atoms. A subsequent combined simulated-annealing downhill simplex and conjugate gradient-optimization procedure gave global minima for mercury clusters with up to 30 atoms. The calculations reveal magic cluster numbers of 6, 13, 19, 23, 26, and 29 atoms. At these cluster sizes, the static dipole polarizability obtained from density-functional theory has a minimum. The calculations also reveal a fast convergence of the polarizability towards the bulk limit in contrast to the singlet-triplet gap or the ionization potential.

DOI: 10.1103/PhysRevLett.89.103401 PACS numbers: 36.40.–c

The simulation of mercury clusters or the bulk is a notoriously difficult problem in computational physics. First, the Hg-Hg interaction is relatively weak (370–400 cm^{-1}) [1] and in the range of typical van der Waals interactions such as Ar_2 (85 cm^{-1}), Kr_2 (127 cm^{-1}), or Xe_2 (186 cm^{-1}) [2]. While two-body potentials for the Group 18 atoms give lattice constants, bulk moduli, and cohesive energies close to the experimental values, a recently derived relativistic coupled-cluster two-body potential for mercury [1] leads to lattice constants $a = b = 3.47(3.46)$ Å, $c = 8.49(6.66)$ Å, and a cohesive energy of $E_{coh} = 0.42(0.79)$ eV for the rhombohedral lattice (experimental values are given in parentheses). For mercury, this implies a rather slow convergence of the n-body expansion of the interaction potential,

$$V = \sum_{i<j} V^{(2)}(r_{ij}) + \sum_{i<j<k} V^{(3)}(r_{ij}, r_{ik}, r_{jk}) + \ldots, \qquad (1)$$

where r_{ij} is the distance between two mercury atoms.

Second, there are currently no quantum theoretical methods available to accurately treat medium to large mercury clusters. Density-functional methods are not accurate enough to treat the dispersive type of interactions [3–5], and coupled-cluster or higher order many-body perturbation theory is too demanding in computer resources. As a further complication, relativistic effects have to be included as well [6]. Even so, solid state calculations for mercury have been performed in the past using density-functional theory (DFT) [6,7], most of them applied experimental lattice parameters and only studied properties of the electronic band structure [8–10]. Using a number of different DFT methods ranging from the local density approximation (LDA) to more sophisticated gradient corrected forms, we obtain lattice parameters and cohesive energies [11] which differ by one order of magnitude; e.g., LDA $a = b = 3.55$ Å, $c = 7.96$ Å, $E_{coh} = 0.67$ eV, PBE [12] $a = b = 3.71$ Å, $c = 9.26$ Å, $E_{coh} = 0.12$ eV, and B3LYP $a = b = 6.26$ Å, $c = 12.24$ Å, $E_{coh} = 0.018$ eV. This is certainly not a very satisfying situation.

The cluster size at which the nonmetal (van der Waals) to metal transition in mercury occurs, that is the band gap ΔE becomes smaller than kT, is still a much debated and controversial issue [13,14]. This transition is estimated to appear at a cluster size of $n \approx 70$ according to Rademann [15], $n \approx 80$ according to Singh [7], $n \approx 135$ according to Pastor *et al.* [16], or even at larger n values [14]. In a recent photoelectron study on negatively charged mercury clusters, the s-p gap was estimated to close at a cluster size of 400 ± 30 [17]. In fluid mercury, the single particle gap between the $6s$ and the $6p$ bands opens at a density of $\rho = 8.8$ g cm^{-3} [18] (compare to 13.59 g cm^{-3} for fluid mercury under standard conditions). It is therefore important to study the band gap in mercury clusters with increasing cluster size.

In order to obtain electronic properties of small to medium-sized mercury clusters, we adopted the following strategy. First, we developed an accurate two-body potential $V^{(2)}$ corrected by basis set superposition errors using relativistic coupled-cluster techniques plus spin-orbit coupling together with correlation consistent basis sets. The computational details are given in Ref. [1]. We then calculated approximately 300 points for the Hg_3 hypersurface at the relativistic second-order many-body perturbation theory level (MBPT2) and adjusted these to a permutation invariant three-body potential $V^{(3)}$ similar to Parish and Dykstra [19]. Coupled cluster calculations at the CCSD(T) level of a few points on the D_{3h} path of the hypersurface ensured that the MBPT2 treatment is sufficiently accurate. Moreover, basis set superposition errors obtained for the three-body part of the potential [20,21] are extremely small and can be neglected; that is, most of the error is contained in the two-body part of the potential which has been removed [1]. We also produced a radially dependent four-body potential along the T_d path of the six-dimensional hypersurface of Hg_4. The results for geometry optimizations up to Hg_5 are shown in Table I in comparison with the pseudopotential results of Flad *et al.* [22].

TABLE I. Bond distance r (in Å), atomization energy D_e (in eV, not corrected for zero-point vibrational energy, ZPVE), and ZPVE (in cm^{-1}) for small mercury clusters dependent on the interaction potential. The symmetries of the global minimum structures are D_{3h} for Hg_3 and Hg_5, and T_d for Hg_4. min/max indicates the smallest and largest Hg-Hg distance in the Hg_5 cluster.

		2	2 + 3	2 + 3 + 4	2 + 3n	Flad *et al.* [22]
r(Hg-Hg)						
Hg_2		3.690	···	···	···	3.75
Hg_3		3.690	3.526	···	3.612	3.75
Hg_4		3.690	3.328	3.355	3.398	3.35
Hg_5	min	3.673	3.287	···	3.361	3.25
	max	5.974	5.424	···	5.530	5.77
D_e						
Hg_2		0.045	···	···	···	
Hg_3		0.136	0.161	···	0.173	0.183
Hg_4		0.180	0.409	0.406	0.403	0.472
Hg_5		0.413	0.690	···	0.628	0.695
ZPVE						
Hg_2		9.8	···	···	···	9.6
Hg_3		29.2	34.8	···	37.1	47.1
Hg_4		57.5	84.5	···	85.5	105.0
Hg_5		87.1	145.0	···	131.3	154.5

The Hg-Hg distances decrease substantially from Hg_2 to Hg_5, and a comparison between the different n-body expansions clearly shows that a two-body potential is not sufficient. By definition, such a potential leads to equal bond distances for the dimer, trimer (equilateral triangle), and the tetramer (tetrahedron). On the other hand, adding the three-body potential leads soon to overbinding for all Hg_n clusters, and we obtain for $n > 7$ bond distances below the solid state value of 2.99 Å. This indicates that higher order body potentials cannot be neglected. Nevertheless, the two- and (2 + 3)-body potentials lead to identical shapes and symmetries for all global minima of Hg_n clusters up to $n = 30$ as our simulating annealing study shows. We therefore adopted a particle dependent three-body potential to account for higher order effects,

$$V^{(3)}(n, r_{ij}, r_{ik}, r_{jk}) = \lambda_n V^{(3)}(r_{ij}, r_{ik}, r_{jk}), \qquad (2)$$

where λ_n is a particle dependent scaling factor such that λ_∞ yields results for the solid state [23] in reasonable agreement with experiment. Test calculations of smaller clusters showed that a linear scaling with inverse cluster size ($\lambda_n = a + bn^{-1}$) is sufficient. We note that shifting the particle dependency from the two- into the three-body part should improve the accuracy. The technical details will be published elsewhere.

Global and close-by local minima for mercury clusters up to Hg_{30} were obtained using a two- plus n-dependent three-body potential (2 + 3n) for mercury in a simulated-annealing treatment combined with a conjugated gradient optimization [24]. From the Hessian, we obtained harmonic frequencies to ensure that all optimized structures are minima on the potential hypersurface. The optimized global minima were used in subsequent DFT calculations applying the local density (LDA) and generalized gradient approximation (B3LYP) [25] to obtain ionization potentials, singlet-triplet gaps, and static dipole polarizabilities for clusters up to Hg_{30} [26].

Figure 1 shows the ionization potentials (IP) at the DFT level together with experimentally obtained values by Cabaud *et al.* [27] and Rademann *et al.* [28]. The experimental values are in between the values obtained by the two DFT methods which gives great confidence for the structures obtained by the (2 + 3n)-body potential. The trend is as one expects for closed-shell interactions. With increasing interaction between the mercury atoms in the cluster, the antibonding highest occupied orbital becomes more diffuse and as a result the IP decreases. We note that the bulk IP is at 4.49 eV [29]. Rademann *et al.* concluded that around Hg_{70} the IPs follow the classical electrostatic behavior for removing an electron from a

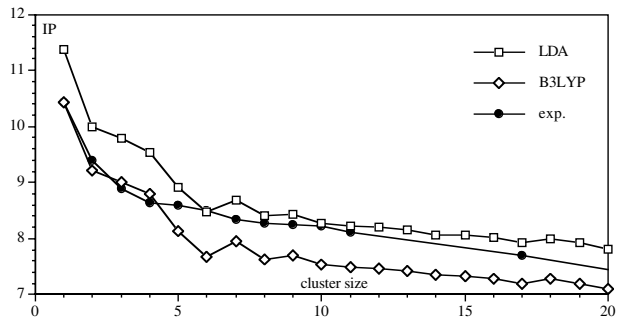

FIG. 1. Ionization potentials IP (in eV) dependent on the cluster size n of Hg_n. Experimental data from Cabaud *et al.* [27] and Rademann *et al.* [28].

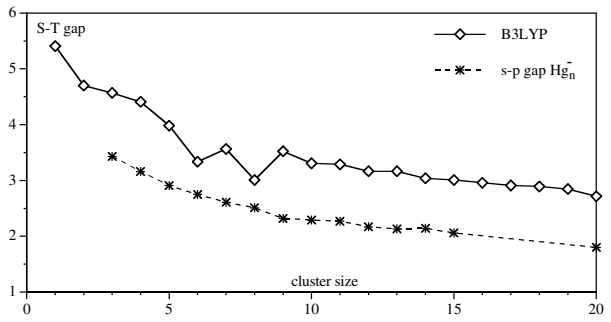

FIG. 2. Singlet-triplet gap (in eV) dependent on the cluster size n of Hg_n. The s-p gap obtained from photoelectron spectra of Hg_n^- clusters [17] is also shown.

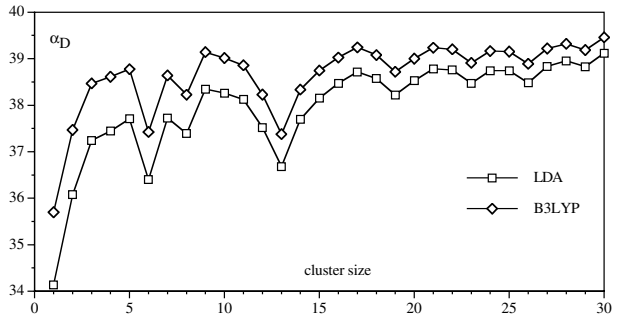

FIG. 3. Static dipole polarizabilities (in a.u.) dependent on the cluster size n of Hg_n.

uniformly conducting sphere. However, our calculated IPs shown in Fig. 1 and the experimentally determined values up to Hg_{70} suggest that convergence towards the bulk limit more likely occurs beyond a few hundred mercury atoms.

Figure 2 shows the calculated singlet-triplet gap for mercury clusters up to Hg_{20}. Again, we see larger variations in the small cluster range up to Hg_9 followed by an almost linear decrease in the singlet-triplet (S-T) gap from Hg_9 to Hg_{20}. Our results are in agreement with the estimated band gap energies of Singh [6]. Extrapolation reveals that the zero gap limit (onset of metallic character) is reached at Hg_{70}. Such an extrapolation is, however, questionable. The data by Busani *et al.* [17] show a change in the behavior of the s-p gap with increasing cluster size at around $n > 15$ which is attributed to a van der Waals to covalent binding transition. Our singlet-triplet gaps are about 1 eV above the data by Busani *et al.* [17], with the overall trend agreeing nicely for a cluster size of ten or larger. The difference between Busani *et al.* and our calculated data is probably mostly due to the fact that different reference states are used, i.e., in the experimental work Hg_n^- was used as the reference state. Hg_n^- is more tightly bound than neutral Hg_n due to charge-induced-dipole interactions. In a simple Franck-Condon picture, we expect that the S-T gaps of the neutral species lie above the photoelectron gap of Hg_n^-. Contraction of the cluster size due to an excess electron of up to 0.35 Å was indeed predicted by Wang *et al.* [30]. This implies that the s-p gap for neutral mercury clusters probably lies above the negatively charged ones thus pushing the metallic limit even further toward larger cluster sizes.

Whilst the IPs and S-T gaps decrease relatively smoothly with increasing cluster size, the calculated dipole polarizabilities show some more detailed features. First, as the IPs decrease with increasing cluster size, the polarizability increases and this overall trend is indeed seen in Fig. 3. On the other hand, it is well known that clusters which form a closed-shell structure within the jellium model (magic numbers, n_{magic}) are least polarizable. Figure 3 indicates that this is the case for $n = 6$, 13, 19, 23, 26, and 29. In fact, these numbers also show up in r_{max}, the maximum Hg-Hg distance in the cluster which increases sharply at $(n_{\text{magic}} + 1)$. Figure 4 shows the structures of these clusters and their high symmetry of either spherical or ellipsoidal shapes. An interesting side aspect is that Hg_{12} does not adopt the high symmetry icosahedral (I_h) structure in contrast to Hg_{13} which includes a central atom. The I_h Hg_{12} structure (which is a local minimum) lies 0.195 eV above the global minimum of C_{5v} symmetry and can be derived from removing an outer Hg atom from the I_h Hg_{13} cluster. We notice that for smaller clusters ($n < 16$) the cluster shapes for the global minima agree with the series of shapes obtained for Morse clusters ($\rho_0 = 6$ in Ref. [31]). Figure 3 also indicates a relatively fast convergence of the dipole polarizability towards the bulk limit which can be estimated to be around 40 a.u. Also the pronounced minima for magic clusters at low cluster size ($n < 15$) smoothes out for larger cluster numbers.

Finally, we show in Fig. 5 the change in energy with increasing cluster size $\Delta E_n = E(n) - E(n-1)$ up to Hg_{30}

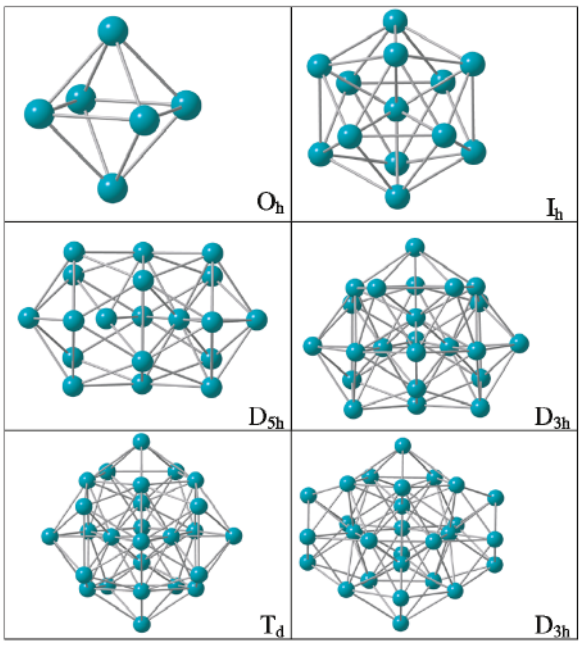

FIG. 4 (color online). Optimized global minima for the clusters with magic number $n = 6$, 13, 19, 23, 26, and 29.

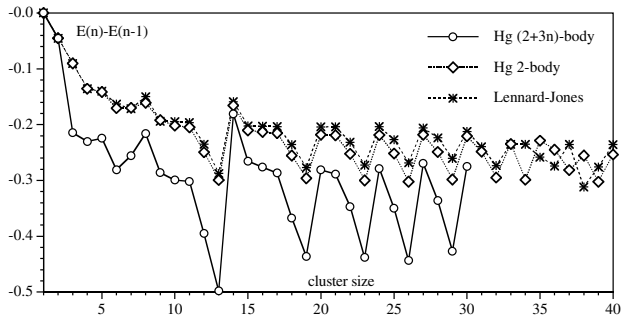

FIG. 5. Change in cluster energy $\Delta E_n = E(n) - E(n-1)$ (in eV) in comparison to a Lennard-Jones behavior [32].

for both the two-body and the $(2 + 3n)$-body potential. It reveals a small minimum at $n = 4$ and minima at the already mentioned cluster sizes of $n = 6$, 13, 19, 23, 26, and 29. For the two-body potential, computational demands are not too high and calculations up to Hg_{40} give further minima in ΔE_n at $n = 32$, 34, 37, and 39. Figure 5 also includes the results for Lennard-Jones clusters [32] which show a remarkably similar behavior to our two-body potential with magic numbers identical up to a cluster size of $n = 32$ [33]. We note that the three-body potential is attractive in the range between 2 and 10 Å. Thus, a comparison between the two-body and $(2 + 3n)$-body potentials shows increased stabilization due to the three-body force for the clusters with magic numbers. Since we have

$$E_{\text{coh}} = \lim_{n\to\infty} \Delta E_n, \tag{3}$$

we observe a relatively slow convergence of ΔE_n towards the bulk cohesive energy [0.61 eV for the $(2 + 3n)$-body potential] according to Fig. 5.

In conclusion, we demonstrated that by using a $(2 + 3n)$-body potential reasonably accurate structures of medium-sized mercury clusters can be predicted which will be useful in future cluster dynamic studies. The most stable structures with increasing cluster size (magic numbers) show up in a pronounced way in the dipole polarizabilities and should be confirmed by future experiments.

We acknowledge the support of the Marsden Fund (Wellington), the Alexander von Humboldt Foundation (Bonn), and the Auckland University Research Committee.

Note added.—While preparing this paper, an article by Hartke, Flad, and Dolg [33] appeared on geometries of smaller Hg clusters up to 14 atoms. Their structures are rather unusual and do not agree with Morse or Lennard-Jones–type structures.

*Email address: schwerd@ccu1.auckland.ac.nz.

[1] P. Schwerdtfeger, R. Wesendrup, G. E. Moyano, A. J. Sadlej, J. Greif, and F. Hensel, J. Chem. Phys. **115**, 7401 (2001).
[2] K. P. Huber and G. Herzberg, *Molecular Spectra and Molecular Structure* (Van Nostrand, New York, 1979), Vol. VI.
[3] E. J. Meijer and M. Sprik, J. Chem. Phys. **105**, 8684 (1996).
[4] X. Wu, M. C. Vargas, S. Nayak, V. Lotrich, and G. Scoles, J. Chem. Phys. **115**, 8748 (2001).
[5] E. Engel, A. Höck, and R. M. Dreizler, Phys. Rev. A **61**, 032502 (2000).
[6] P. P. Singh, Phys. Rev. Lett. **72**, 2446 (1994).
[7] P. P. Singh, Phys. Rev. B **49**, 4954 (1994).
[8] S. C. Keeton and T. L. Louks, Phys. Rev. **152**, 548 (1966).
[9] L. F. Mattheiss and W. W. Warren, Jr., Phys. Rev. B **16**, 624 (1977).
[10] S. Deng, A. Simon, and J. Köhler, Angew. Chem., Int. Ed. Engl. **37**, 640 (1998).
[11] V. R. Saunders *et al.*, program CRYSTAL98, University of Torino, Torino, 1998.
[12] J. P. Perdew, K. Burke, and M. Ernzerhof, Phys. Rev. Lett. **77**, 3865 (1996).
[13] R. L. Johnston, Philos. Trans. R. Soc. London A **356**, 211 (1998).
[14] H. Haberland, B. von Issendorff, Ji Yufeng, T. Kolar, and G. Thanner, Z. Phys. D **26**, 8 (1993).
[15] K. Rademann, Z. Phys. D **19**, 161 (1991).
[16] G. M. Pastor, P. Stampfli, and K. H. Bennemann, Phys. Scr. **38**, 623 (1988).
[17] R. Busani, M. Folkers, and O. Cheshnovsky, Phys. Rev. Lett. **81**, 3836 (1998).
[18] G. Kresse and J. Hafner, Phys. Rev. B **55**, 7539 (1997).
[19] C. A. Parish and C. E. Dykstra, J. Chem. Phys. **98**, 437 (1993).
[20] P. Valiron and I. Mayer, Chem. Phys. Lett. **275**, 46 (1997).
[21] S. F. Boys and F. Bernardi, Mol. Phys. **19**, 553 (1970).
[22] H.-J. Flad, F. Schautz, Y. Wang, M. Dolg, and A. Savin, Eur. Phys. J. D **6**, 243 (1999).
[23] P. Schwerdtfeger, program SAMBA, The University of Auckland, Auckland, 2001.
[24] G. Moyano, M. Pernpointner, and P. Schwerdtfeger, program MAMBO, The University of Auckland, Auckland, 2001.
[25] *Recent Developments and Applications of Modern Density-Functional Theory, Theoretical and Computational Chemistry*, edited by J. M. Seminario (Elsevier, Amsterdam, 1996).
[26] M. J. Frisch *et al.*, program GAUSSIAN98, Gaussian Inc., Pittsburgh, PA, 1998.
[27] B. Cabaud, A. Hoareau, and P. Melinon, J. Phys. D **13**, 1831 (1980).
[28] K. Rademann, B. Kaiser, U. Even, and F. Hensel, Phys. Rev. Lett. **59**, 2319 (1987).
[29] P. Cotti, H.-J. Güntherodt, P. Munz, P. Oelhafen, and J. Wullschleger, Solid State Commun. **12**, 635 (1973).
[30] Y. Wang, H.-J. Flad, and M. Dolg, Int. J. Mass Spectrom. **201**, 197 (2000).
[31] J. P. K. Doye, D. J. Wales, and R. S. Berry, J. Chem. Phys. **103**, 4234 (1995).
[32] D. J. Wales and J. P. K. Doye, J. Phys. Chem. A **101**, 5111 (1997).
[33] B. Hartke, H.-J. Flad, and M. Dolg, Phys. Chem. Chem. Phys. **3**, 5121 (2001).